The new heavy fermion compound $Ce_3Bi_4Ni_3$

D. M. Kirschbaum,[1] X. Yan,[1] M. Waas,[1] R. Svagera,[1] A. Prokofiev,[1]
B. Stöger,[2] P. Rogl,[3] D.-G. Oprea,[4,5] C. Felser,[4] R. Valentí,[5] M.
G. Vergniory,[4,6] J. Custers,[7] S. Paschen,[1,*] and D. A. Zocco[1,†]

[1]*Institute of Solid State Physics, Vienna University of Technology, 1040 Vienna, Austria*
[2]*X-ray Center, Vienna University of Technology, 1040 Vienna, Austria*
[3]*Institute of Materials Chemistry, University of Vienna, 1090 Vienna, Austria*
[4]*Max Planck Institute for Chemical Physics of Solids, 01187 Dresden, Germany*
[5]*Institute for Theoretical Physics, Goethe University*
Frankfurt, 60438 Frankfurt a.M., Germany
[6]*Donostia International Physics Center,*
20018 Donostia–San Sebastian, Spain
[7]*Dept. of Condensed Matter Physics,*
Charles University, 121 16 Prague, Czech Republic

(Dated: November 30, 2023)

Abstract

The family of cubic noncentrosymmetric 3-4-3 compounds has become a fertile ground for the discovery of novel correlated metallic and insulating phases. Here, we report the synthesis of a new heavy fermion compound, $Ce_3Bi_4Ni_3$. It is an isoelectronic analog of the prototypical Kondo insulator $Ce_3Bi_4Pt_3$ and of the recently discovered Weyl-Kondo semimetal $Ce_3Bi_4Pd_3$. In contrast to the volume-preserving Pt-Pd substitution, structural and chemical analyses reveal a positive chemical pressure effect in $Ce_3Bi_4Ni_3$ relative to its heavier counterparts. Based on the results of electrical resistivity, Hall effect, magnetic susceptibility, and specific heat measurements, we identify an energy gap of 65–70 meV, about 8 times larger than that in $Ce_3Bi_4Pt_3$ and about 45 times larger than that of the Kondo-insulating background hosting the Weyl nodes in $Ce_3Bi_4Pd_3$. We show that this gap as well as other physical properties do not evolve monotonically with increasing atomic number, i.e., in the sequence $Ce_3Bi_4Ni_3$-$Ce_3Bi_4Pd_3$-$Ce_3Bi_4Pt_3$, but instead with increasing partial electronic density of states of the d orbitals at the Fermi energy. To understand under which condition topological states form in these materials is a topic for future studies.

I. INTRODUCTION

The prospect that strong electron correlations and nontrivial electronic topology could cooperate in the formation of novel quantum states of matter has sparked great interest in recent years. Much attention has been given to heavy fermion materials, with proposals to realize correlated topological states in Kondo insulators and semimetals [1–3]. In the family of cubic, noncentrosymmetric Ce-based "3-4-3" compounds of space group 220, $Ce_3Bi_4Pt_3$ is perhaps the best-known case. It was classified early on as a Kondo insulator (KI) [4–6], a material where the Kondo interaction between localized (typically $4f$) states and conduction electrons (typically from d shells) promotes the formation of a narrow band gap [7]. More recently it was found that the isoelectronic and isosize substitution of Pt by Pd consecutively reduces the gap, ultimately giving rise to a novel Weyl-Kondo semimetal (WKSM) state in the end compound $Ce_3Bi_4Pd_3$ [8–10].

Magnetic field experiments showed that the WKSM (gapless) signatures observed in

* Corresponding author: paschen@ifp.tuwien.ac.at

† Corresponding author: zocco@ifp.tuwien.ac.at

$Ce_3Bi_4Pd_3$ can be readily suppressed at a modest field of 9 T while maintaining the Kondo interaction essentially intact [11–13]. The background Kondo gap, albeit small, remains finite up to a considerably larger magnetic field, as demonstrated from magnetic torque and susceptibility experiments [11, 14]. High pressure studies indicate that a larger gap value similar to that of $Ce_3Bi_4Pt_3$ is gradually recovered [15]. Yet, a detailed understanding of how the WKSM state is affected by volume and hybridization changes produced by chemical substitutions [8, 16] or externally applied pressure [15, 17, 18] is currently lacking.

Here we extend the previous isoelectronic substitution study ($5d$ to $4d$) one step further, to the Ni case ($3d$). We present the synthesis of high-quality single crystals of $Ce_3Bi_4Ni_3$, a material that has not been synthesized in any form before. Structural analysis reveals that the Ni substitution results in a positive chemical pressure, distinct from the volume-preserving Pt-Pd substitution, which gives new insight into the pressure effects on $Ce_3Bi_4Pd_3$. Electrical resistivity, Hall effect, magnetic susceptibility, and specific heat measurements suggest that $Ce_3Bi_4Ni_3$ is a new heavy fermion compound with a hybridization gap that is large compared to those of the Pd and Pt compounds. We end by discussing the evolution of the characteristic energy scales across the $Ce_3Bi_4X_3$ series (X = Ni, Pd, Pt), and relate it to the results of electronic band structure calculations.

II. SINGLE CRYSTAL GROWTH AND CHARACTERIZATION

Materials with the chemical formula $R_3Pn_4X_3$, where R is a rare earth or actinide element, Pn is a pnictide (As, Sb, Bi), and X is a transition metal element, have been investigated for decades [19–22]. Among the Ce compounds, the Kondo insulator $Ce_3Bi_4Pt_3$ has been known for decades [4–6]. Single crystals of the isoelectronic compound $Ce_3Bi_4Pd_3$ were recently obtained via the Bi-flux technique [8], but the synthesis of the Ni phase has remained elusive so far. Our initial attempts to prepare polycrystalline samples confirmed that the $Ce_3Bi_4Ni_3$ phase indeed forms, and encouraged us to attempt single crystal growth using various fluxes. A detailed description of the sample synthesis is presented in Appendix A.

Single crystals of $Ce_3Bi_4Ni_3$ with faceted surfaces and maximum sizes of $2 \times 0.5 \times 0.5\,\mathrm{mm}^3$ were successfully grown using Pb flux [Fig. 1(a)]. Laue X-ray diffraction (XRD) provides clear patterns, confirming the high quality of the crystals [Fig. 1(b)]. Similarly to the Pt and Pd 3-4-3 compounds, the powder and single-crystal XRD data of $Ce_3Bi_4Ni_3$ can be

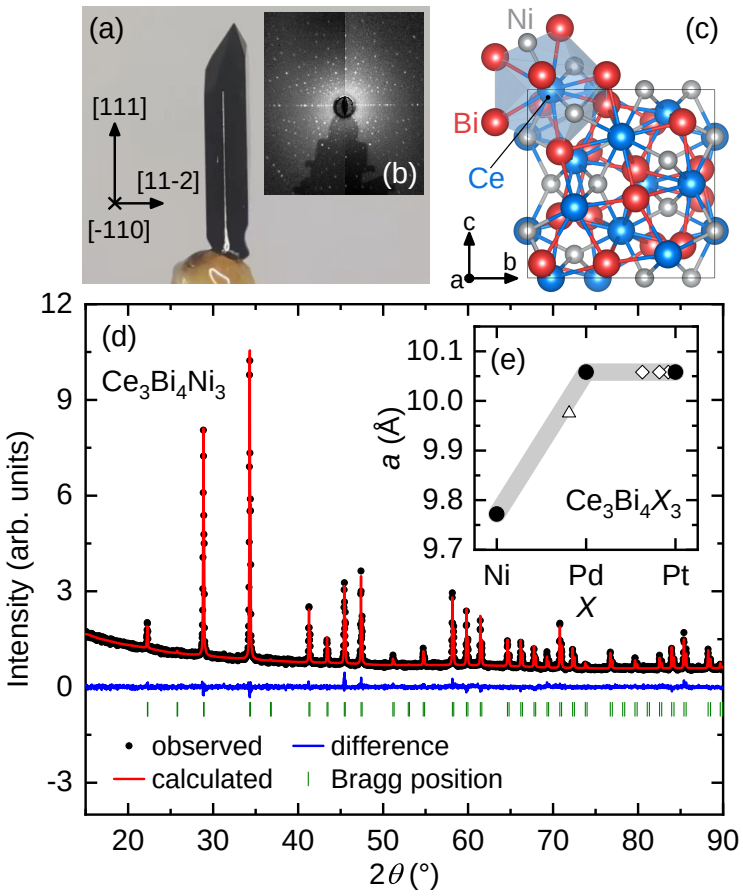

FIG. 1. **(a)** Photo of a single crystal of $Ce_3Bi_4Ni_3$ with indicated crystallographic directions obtained from Laue diffraction. Typical sample length is 1.5 mm. **(b)** Laue XRD pattern (white spots). The center of the image corresponds to the [-2, -1, -1] crystallographic direction. **(c)** Sketch of the unit cell. The polyhedron emphasizes the close environment of a Ce atom. **(d)** Room-temperature powder XRD pattern of $Ce_3Bi_4Ni_3$ (black dots). Vertical bars indicate the positions of the expected diffraction peaks. The difference (blue line) between the measured data and the refinement (red line) shows no signs of impurity phases. **(e)** Lattice parameter a across the $Ce_3Bi_4(Ni,Pd,Pt)_3$ series. Intermediate Pd-Pt values (white diamonds) taken from Ref. [8]. The grey shaded line is a guide to the eye.

refined with the cubic $Y_3Sb_4Au_3$ structure, space group 220, $I\bar{4}3d$ [19, 23]. The unit cell contains 4 formula units, with 40 atoms forming a noncentrosymmetric structure. Figure 1(c) displays the crammed unit cell; the local environment of a Ce atom is comprised of 8 Bi atoms and 4 Ni atoms (nearest neighbors, see Appendix B, Table B). Rietveld refinements of the powder XRD data of the most stoichiometric samples [Fig. 1(d)] yield an average room-

temperature lattice parameter $a = 9.7715(9)$ Å (see Appendix C). The unit cell volume of $Ce_3Bi_4Ni_3$ is therefore compressed by $\sim 8\%$ with respect to the (essentially isovolume [8]) Pt ($a = 10.051$ Å) and Pd ($a = 10.058$ Å) compounds [Fig. 1(e)]. These results were confirmed and studied in more detail with single crystal XRD experiments performed at 100 K, 200 K, and 300 K. A summary of the structural data obtained from a highly stoichiometric sample, including interatomic distances, atomic occupancies, and atomic displacement parameters (ADPs), is presented in Appendix B.

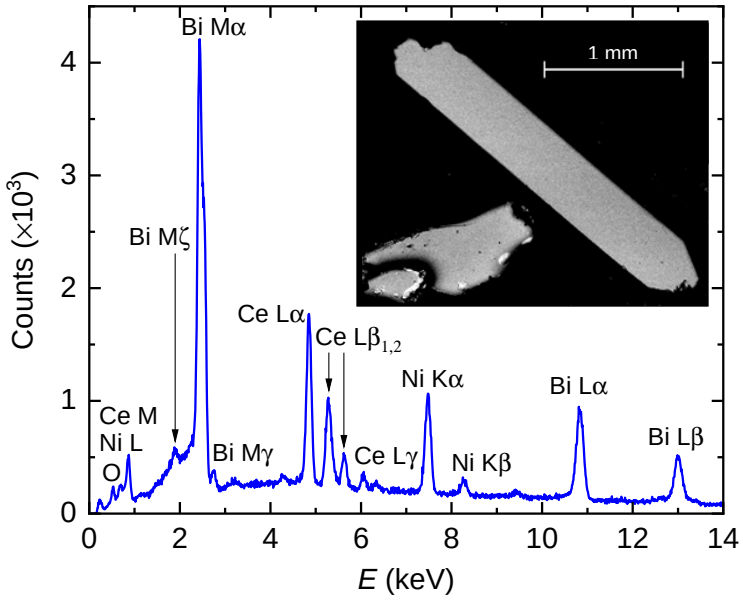

FIG. 2. EDX spectrum corresponding to one point measurement of a polished $Ce_3Bi_4Ni_3$ crystal (inset, top right). Inset: backscattered SEM images of as-grown (bottom left) and polished (top right) $Ce_3Bi_4Ni_3$ samples. The lighter spots visible in the as-grown crystal correspond to Pb inclusions, and are absent in the polished sample.

The stoichiometries of the samples were determined via energy dispersive X-ray spectroscopy (EDX) after each growth campaign. Figure 2 displays a representative EDX spectrum collected from the polished surface of a high-quality single crystal. The mean composition $Ce_{3.15(5)}Bi_{3.90(9)}Ni_{2.94(4)}$ was obtained from spectra taken at 6 different spots of a sample. Scanning electron microscopy (SEM) images obtained from as-grown single crystals (inset of Fig. 2, bottom left) show lighter spots, which could originate from residual flux solidifying after centrifuging. In high-quality single crystals, these inclusions are only present at the surface of the samples, and can therefore be removed by etching with hydrogen peroxide

(H_2O_2) and careful polishing (inset of Fig. 2, top right). Spurious superconductivity can therefore be prevented or eliminated, as we confirm by magnetic susceptibility and electrical resistivity measurements. A possible substitution of Bi by Pb in $Ce_3Bi_4Ni_3$ has been ruled out by comparing the EDX spectra of a Pb-flux grown single crystal and that of a Pb-free annealed polycrystalline sample.

Samples of $Ce_3Bi_4Ni_3$ are sensitive to air and moisture. A distinct degradation of the powder XRD intensity was observed after a 5 h exposure of the powder to air. The oxygen contamination can also be detected in the EDX spectrum after a short exposure time (small peak in the low energy region of Fig. 2).

From a combined analysis of the EDX, powder XRD, and magnetic susceptibility measurements, we can select with good certainty the most stoichiometric, high-quality single crystals. A detailed discussion of this analysis is presented in Appendix C. In the following sections we present the physical properties of $Ce_3Bi_4Ni_3$ corresponding to samples with Ni content closest to 3 atoms per mol.

III. PHYSICAL PROPERTIES

The electrical resistivity $\rho(T)$ of $Ce_3Bi_4Ni_3$ is displayed in Fig. 3(a). Similarly to the Pt and Pd 3-4-3 compounds, nonmetallic behavior is observed across the entire studied temperature range (a detailed comparison is presented in Section IV). ρ increases by more than two orders of magnitude from room temperature to 2 K, with a resulting inverse residual resistivity ratio $iRRR = \rho(2\,\mathrm{K})/\rho(300\,\mathrm{K}) = 440$. Above 100 K, $\rho(T)$ can be well described by a thermally activated scattering process across a gap. At lower temperatures, the systems enters a regime where the increase in resistivity with decreasing temperature is less pronounced. First, a shoulder develops at approximately 50 K, followed by a second, low-temperature thermally activated regime between 10 K and 30 K. A small energy gap of $\sim$20 K could be extracted from this narrow temperature range, although one might argue that other effects, such as the presence of in-gap states, could be responsible for this particular temperature dependence of the resistivity. Finally, $\rho(T)$ begins to flatten below 10 K, but without reaching saturation down to 2 K.

Figure 3(b) displays the temperature evolution of the Hall coefficient R_H, obtained from linear fits to the low-field region of isothermal Hall resistivity curves (linear in $B \leq 9$ T

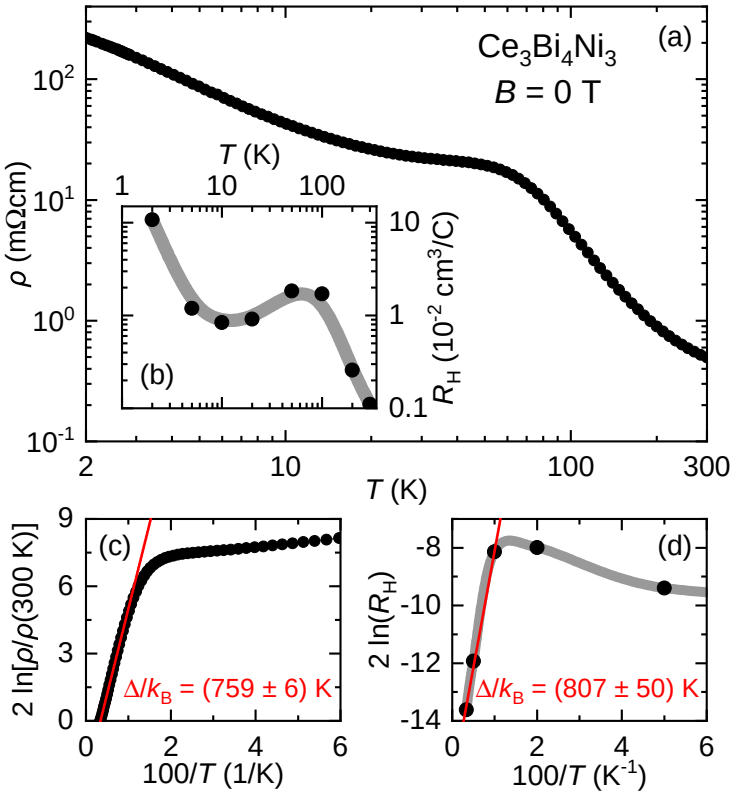

FIG. 3. **(a)** Electrical resistivity ρ of $Ce_3Bi_4Ni_3$ as a function of temperature T in zero magnetic field. **(b)** Temperature-dependent Hall coefficient R_H. The shaded grey line is a guide to the eye. **(c),(d)** Arrhenius plots of the resistivity (normalized to 300 K) and Hall coefficient data. The red solid lines are linear fits to the data above 100 K.

for $10\,\mathrm{K} \leq T \leq 300\,\mathrm{K}$). $R_H(T)$ reaches a local maximum near 50 K and tends to saturate at lower temperatures. This peak coincides with the end of the thermally activated regime. The increase of $R_H(T)$ below 10 K might be due to the freezing out of thermally activated carriers from shallow in-gap states, the origin of which needs further investigation.

To determine the size of the gap Δ, the transport data are fitted with thermally activated behavior, $\rho = \rho_0 \exp[\Delta/(2k_BT)]$ and $R_H = R_{H,0} \exp[\Delta/(2k_BT)]$, as shown in Arrhenius plots [Fig. 3(c, d)]. Δ values of 759 K and 807 K are obtained from the fits of the resistivity and Hall coefficient above 100 K, respectively. These values are 7–10 times larger than the values reported for $Ce_3Bi_4Pt_3$ [5, 8] and at least 45 times larger than the Kondo gap acting on the background of the WKSM state of $Ce_3Bi_4Pd_3$ in the absence of applied magnetic field [8, 11], suggesting the presence of a much larger Kondo energy scale at play in the Ni compound.

The magnetic susceptibility $\chi(T)$ of $Ce_3Bi_4Ni_3$ displays a broad maximum at $T^{\chi}_{\mathrm{max}} = 280\,\mathrm{K}$

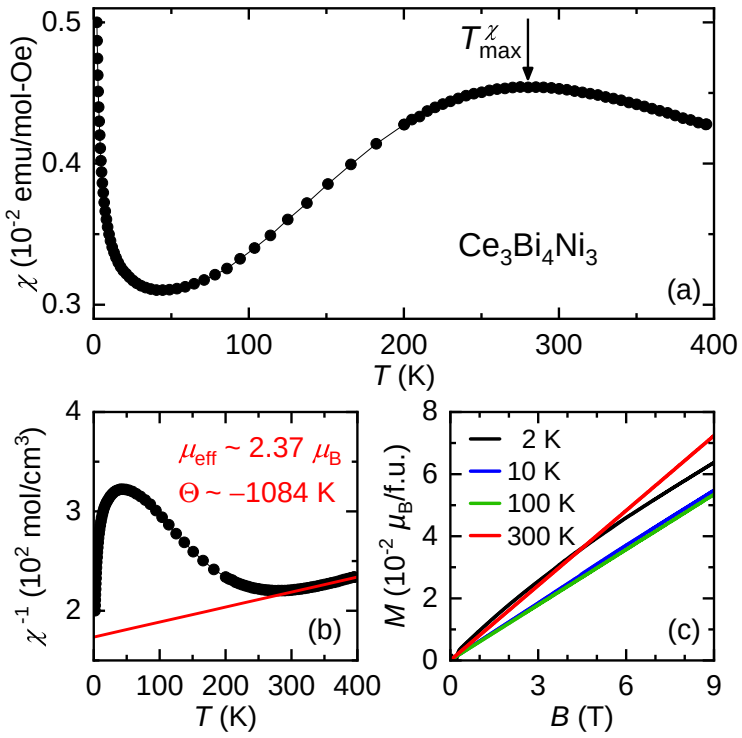

FIG. 4. **(a)** Temperature dependence of the magnetic susceptibility χ of $Ce_3Bi_4Ni_3$, measured with $B = 1\,\mathrm{T}$. **(b)** Inverse magnetic susceptibility $\chi^{-1}(T)$. The paramagnetic Weiss temperate Θ and the effective magnetic moment μ_{eff} were determined from a Curie-Weiss fit for $T > T^{\chi}_{\mathrm{max}}$ (red line). **(c)** Magnetization M vs B at 2 K (black), 10 K (blue), 100 K (green) and 300 K (red). The curves show up and down B-sweeps, with no signs of magnetic hysteresis detected.

[Fig. 4(a)]. In Kondo insulators, the occurrence of such maxima has been associated with the onset of Kondo screening and the opening of a hybridization gap [7]. We estimate a Kondo temperature using the Kondo lattice expression $T_{\mathrm{K}} \approx 4T^{\chi}_{\mathrm{max}}/(2J+1) = 187\,\mathrm{K}$ [5, 24], with a total angular momentum $J = 5/2$ for Ce^{3+}. The upturn in χ vs T observed at lower temperatures is generally attributed to small amounts of magnetic impurities or defects [25] which were not detected in our XRD experiments. Assuming Curie-Weiss behavior for $T > T^{\chi}_{\mathrm{max}}$, a linear fit to the inverse susceptibility $\chi^{-1}(T)$ in the limited available temperature range [Fig. 4(b)] yields a large negative Weiss temperature $\Theta \sim -1084\,\mathrm{K}$ —typical for Kondo insulators— and an effective magnetic moment $\mu_{\mathrm{eff}} \sim 2.37\mu_{\mathrm{B}}$, slightly reduced from the Hund's rules value of $2.54\mu_{\mathrm{B}}$ for free Ce^{3+} ions.

The magnetization curves $M(B)$ are linear in field at 10 K, 100 K, and 300 K [Fig. 4(c)]. A slight curvature appears only in the 2 K measurement, without reaching saturation up

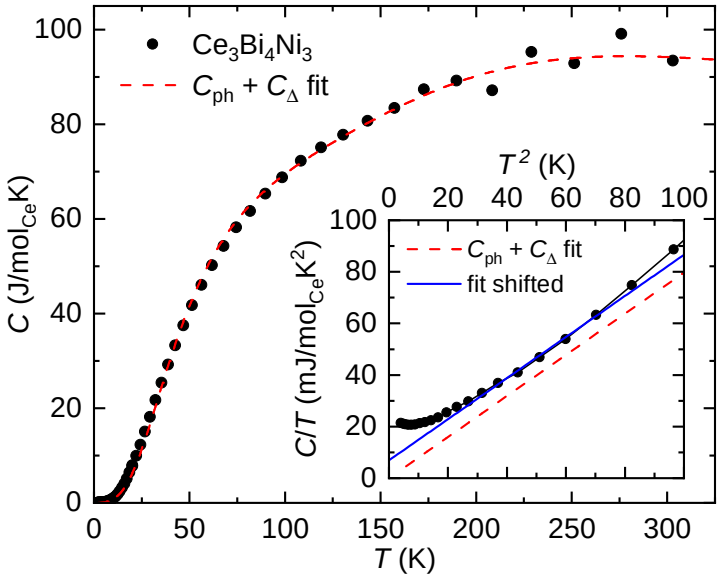

FIG. 5. Specific heat C vs T of $Ce_3Bi_4Ni_3$ measured between 2 K and 300 K. The red dashed line is a fit with the Debye model plus an additional Schottky-like electronic contribution derived for Kondo insulators (see main text). The inset shows the low temperature C/T vs T^2 and the fit. The Sommerfeld coefficient (γ) is then determined by shifting the fitting line by $\gamma = 6.92\,\mathrm{mJ/mol_{Ce}K^2}$ to match the measured data (blue line).

to 9 T. No indications of magnetic hysteresis were observed in any of the measurements. Overall, $Ce_3Bi_4Ni_3$ appears to be well described as a paramagnetic Kondo insulator, without magnetic ordering down to 2 K.

We can gain further understanding on the nature of the ground state of $Ce_3Bi_4Ni_3$ and the strength of the Kondo interaction from the specific heat $C(T)$ measurements presented in Fig. 5. So far, our efforts to synthesize $La_3Bi_4Ni_3$ as a non-f-electron reference compound have been unsuccessful. To isolate the electronic and magnetic (Ce $4f$ related) contributions to the specific heat, we therefore model the data as $C(T) = \gamma T + C_{\mathrm{ph}} + C_\Delta$. The first term is the linear-in-temperature electronic (Sommerfeld) contribution, the second term the phonon specific heat described by the Debye model [26]. C_Δ accounts for an additional Schottky-like electronic contribution in Kondo insulators, which has previously been modelled with two sharp peaks in the density of states, located above and below the energy gap [7]:

$$C_\Delta \propto \left(\frac{\Delta}{2k_\mathrm{B}T}\right)^2 \frac{(2J+1)\exp\left[\Delta/2k_\mathrm{B}T\right]}{\left(2J+1+\exp\left[\Delta/2k_\mathrm{B}T\right]\right)^2}\,. \tag{1}$$

The contribution from the Sommerfeld term is expected to be very small. In addition,

its extraction is complicated by a low-temperature upturn in C/T (see inset of Fig. 5). We therefore set $\gamma = 0$ and fit the data above 20 K using the full Debye integral. The fit yields a Debye temperature $\Theta_D = (202 \pm 3)$ K and a large gap $\Delta = (1693 \pm 87)$ K, consistent with the large value of T^{χ}_{max} presented above. We can nevertheless obtain an estimate of the Sommerfeld coefficient γ by matching the fit to the measured data in a C/T vs T^2 plot at low temperatures (blue line in inset of Fig. 5). The required shift along the C/T axis then corresponds to $\gamma = 6.92\,\mathrm{mJ/mol_{Ce}K^2}$, similarly small to the value determined for $Ce_3Bi_4Pt_3$ [5]. $Ce_3Bi_4Ni_3$ displays a small low-temperature upturn visible in C/T which could be due to magnetic impurities, as we previously discussed for the magnetic susceptibility data (Fig. 4). However, the upturn could also be related to the onset of non-Fermi liquid behavior in the presence of a nearby quantum critical point. Additional low-temperature investigations are needed to unveil its true origin.

IV. DISCUSSION

We can now take a look at $Ce_3Bi_4Ni_3$ in the context of the $Ce_3Bi_4X_3$ series (X = Ni, Pd, Pt). The lattice parameters a for the three compounds are shown in Fig. 1(e). In addition, we include the values corresponding to the intermediate Pt-Pd substitution $Ce_3Bi_4(Pt_{1-x}Pd_x)_3$ from Ref. [8] and one value corresponding to the intermediate Pd-Ni substitution $Ce_3Bi_4(Pd_{1-x}Ni_x)_3$ with $x = 0.19$. Unlike the Pt-Pd case, which appears to exert very little to no-effect on the unit cell volume [8], the substitution of Pd with Ni is no longer isosize. In this context, chemical (and, possibly, external) pressure becomes now a relevant parameter for tuning the Kondo coupling J_K across the extended Ce 3-4-3 series.

A recent study on the electronic transport properties of $Ce_3Bi_4Pd_3$ under hydrostatic pressure showed that the energy gap extracted from resistivity increases quadratically with applied pressure, reaching a value of ~ 4.8 meV at 2.3 GPa [15, 27]. Hence, pressure appears to drive $Ce_3Bi_4Pd_3$ to a more insulating state. In this work [15], as well as in two recent theoretical studies [17, 18], it was thus argued that pressure drives $Ce_3Bi_4Pd_3$ towards $Ce_3Bi_4Pt_3$, which, at that point, was the only known isoelectronic compound of this series. In view of the chemical pressure effect presented in Fig. 1(e), here we argue that, instead, pressure drives $Ce_3Bi_4Pd_3$ towards the Ni compound. We can translate the 8.3% shrinking of the unit cell volume obtained from $Ce_3Bi_4Pd_3$ to $Ce_3Bi_4Ni_3$ to an equivalent externally

applied pressure P using the third-order Birch-Murnaghan equation of state [28]

$$P(V) = \frac{3B_0}{2}\left[\left(\frac{V_0}{V}\right)^{\frac{7}{3}} - \left(\frac{V_0}{V}\right)^{\frac{5}{3}}\right] \times \left\{1 + \frac{3}{4}(B_0' - 4)\left[\left(\frac{V_0}{V}\right)^{\frac{2}{3}} - 1\right]\right\}, \qquad (2)$$

where V_0 is the ambient pressure volume, V is the compressed volume, B_0 is the bulk modulus, and B_0' its derivative with respect to pressure. B_0 and B_0' result typically from fits to $V(P)$ data obtained in high-pressure X-ray diffraction experiments. Since such data are not yet available for $Ce_3Bi_4Pd_3$, we use the values $B_0 = 59.1\,\text{GPa}$ and $B_0' = 6.9$ reported for the isostructural (and isosize) compound $Ce_3Bi_4Pt_3$ [29], which provide also a good agreement with the pressure-dependent unit cell parameters calculated via DFT+U [18]. This calculation yields a pressure of 6.9 GPa equivalent to the compression effect resulting from the Pd-Ni substitution. Using the quadratic dependence of $\Delta(P)$ from the experiments reported in Ref. [15, 27], a pressure of 9.4 GPa would then be necessary to reach the energy gap value estimated for $Ce_3Bi_4Ni_3$ (Fig. 3), close to the value calculated using the Birch-Murnaghan formula.

In Fig. 6 we compare the normalized resistances $R(T)/R(300\,\text{K})$ and magnetic susceptibilities of the Ni, Pd, and Pt compounds. Perhaps surprisingly at first sight, the transport and magnetic properties of this isoelectronic series evolve nonmonotonically with atomic number. The $iRRR$ decreases by more than 2 orders of magnitude from $Ce_3Bi_4Ni_3$ to $Ce_3Bi_4Pd_3$, and recovers the value of the Ni compound when Pd is substituted by Pt. A slight change in resistivity from the pure Pd compound is already evident when Pd is substituted by 19% Ni [blue line vs white triangles in Fig. 6(a)]. Similarly, the characteristic peak in susceptibility at T^{χ}_{max} [indicated by arrows in Fig. 6(b)] shifts first from room temperature to $\sim 12\,\text{K}$ from the Ni to the Pd compound, and increases back to $\sim 75\,\text{K}$ for $Ce_3Bi_4Pt_3$.

To help visualizing the evolution across the series, we present in Fig. 7(a) (notice the logarithmic vertical axis) the values of T^{χ}_{max} and $iRRR$ extracted from Fig. 6, together with the values Δ/k_{B} and T_{K} obtained as described in Section III. As we mentioned earlier, the transport properties of $Ce_3Bi_4Pd_3$ at low temperatures and zero magnetic field are largely dominated by the effects of the gapless WKSM ground state [8, 10, 11]. For this reason, as noted in Ref. [8], the finite energy gap value of 16.9 K for $Ce_3Bi_4Pd_3$ obtained via Arrhenius fits to the $B = 0$ resistivity data should be taken with caution, and therefore it is presented as a shaded/dotted line symbol in Fig. 7. Nevertheless, the value is in good agreement with magnetic field-derived energy of $\sim 1.5\,\text{meV}$ required to close the Kondo gap [11].

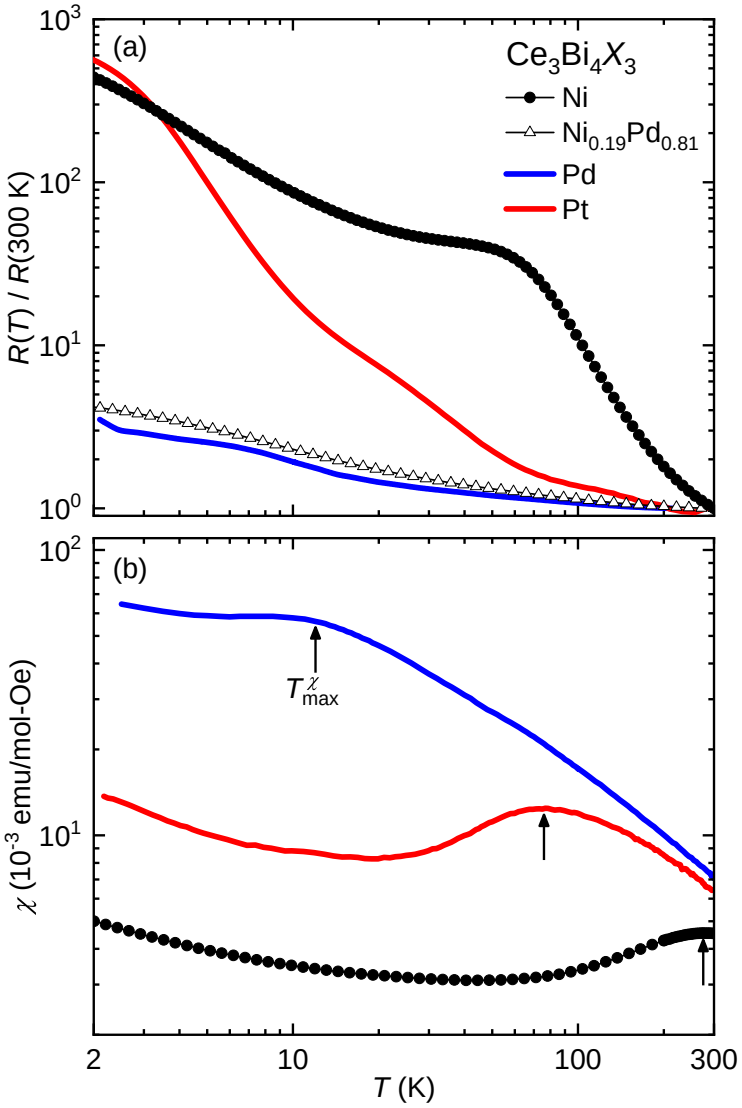

FIG. 6. **(a)** Electrical resistance $R(T)$ normalized to its room temperature value $R(300\,\mathrm{K})$ and **(b)** magnetic susceptibility $\chi(T)$ of the $Ce_3Bi_4X_3$ series, with X = Ni (black dots), Pd (blue line), Pt (red line), and of a partially Ni-Pd single crystal (19% Ni, white triangles). The data for $Ce_3Bi_4Pd_3$ and $Ce_3Bi_4Pt_3$ were taken from Refs. [8] and [10].

Overall, the nonmonotonic change of the characteristic parameters form a "U" shape centered around the most strongly correlated material in the series $Ce_3Bi_4Pd_3$, and with the comparably less correlated, large Kondo-gap compounds $Ce_3Bi_4Pt_3$ and $Ce_3Bi_4Ni_3$ lying at either side. While pressure arguments alone could suffice, as discussed above, to broadly describe the Ni-Pd side of this plot, they cannot explain the changes in Kondo coupling observed under the volume-preserving Pd-Pt substitution, and, therefore, other arguments

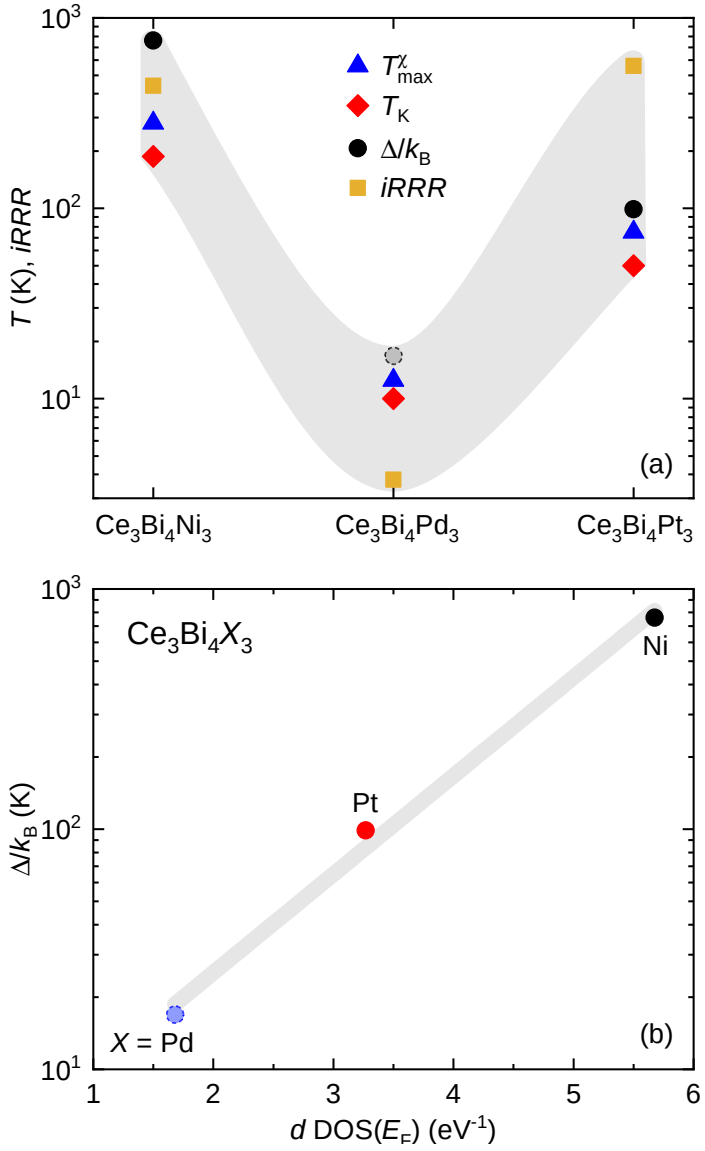

FIG. 7. Comparison of characteristic parameters for the $Ce_3Bi_4X_3$ series (X = Ni, Pd, Pt). Shaded grey areas are guides to the eyes. **(a)** $iRRR$ values (from Fig. 6) and temperature scales T_K, Δ/k_B, and T^{χ}_{max}. For $Ce_3Bi_4Ni_3$, T^{χ}_{max} is taken from Fig. 4(a), T_K is calculated from T^{χ}_{max} (see Section III), and Δ/k_B is obtained from the fits in Figs. 3(c-d). Values for the Pd and Pt compounds taken from Ref. [8]. **(b)** Kondo energy gap Δ/k_B as a function of the d-electron density of states (d DOS) at the Fermi level (from DFT calculations, see Appendix D).

are necessary to understand the entire nonmonotonic evolution found across the series. A recent analysis of electronic band structure calculations suggested that the radial extension of the d orbitals could play an important role in the determination of the Kondo coupling in

these hybridization-gapped materials [16]. Our density functional theory (DFT) calculations of the whole series appears to confirm this hypothesis. The aim of these calculations is to extract the d-electron density of states at the Fermi level, a key factor determining the Kondo interaction strength. As the Kondo effect itself cannot be captured by DFT, the $4f$ electron of Ce is treated as core electron (see Appendix D for more details). Figure 7(b) displays the Kondo scale Δ/k_{B} as a function of the d-orbital electron density of states ($d\,\mathrm{DOS}$) at the Fermi level for the three $Ce_3Bi_4X_3$ compounds (see Appendix D). The Kondo scale increases exponentially with the $d\,\mathrm{DOS}(E_{\mathrm{F}})$ (shaded grey line in the semi-log plot), but it does it nonmonotonically with the principal atomic number n, increasing from the Pd $4d$ to the Pt $5d$ compounds, and reaching its maximum for the $3d$ $Ce_3Bi_4Ni_3$. Hence, we conclude that the nonmonotonic evolution of the physical properties across the isoelectronic series can be explained by the relationship between Kondo coupling and d-orbital density of states.

V. CONCLUSIONS

In summary, we successfully synthesized single crystals of $Ce_3Bi_4Ni_3$ using Pb flux. The high quality of the samples was verified via XRD and EDX measurements. From electrical resistivity, Hall effect, magnetic susceptibility, and specific heat experiments, we conclude that $Ce_3Bi_4Ni_3$ is a paramagnetic heavy fermion material with a relatively large Kondo gap of 65–70 meV. In the context of the $Ce_3Bi_4X_3$ series (X = Ni, Pd, Pt) we find a positive chemical pressure effect in $Ce_3Bi_4Ni_3$ relative to the heavier Pd and Pt compounds. Notably, the transport and magnetic properties as well as the extracted characteristic energy scales evolve nonmonotonically throughout this isoelectronic series. We attribute this behavior to the nonmonotonic variation of d-orbital DOS at the Fermi level. Obtaining a detailed understanding of how the variations in orbital hybridization affect the Kondo coupling across the Ni-Pd-Pt isoelectronic series would have a broader impact for future experimental and theoretical studies. For example, the giant topological responses found in various physical properties of $Ce_3Bi_4Pd_3$ arise from strongly renormalized Weyl bands located within a Kondo insulating gap [8–10], which in turn acts in the background as a shield against the effects of topologically trivial bands. It would then be interesting to explore how the WKSM signatures observed in $Ce_3Bi_4Pd_3$ will evolve as the band structure is carefully tuned via

various Ni-Pd-Pt substitutions, and as a function of externally applied pressure.

ACKNOWLEDGMENTS

The work in Vienna was supported by the Austrian Science Fund (FWF projects I 4047-N27 and I 5868-FOR 5249 - QUAST), the European Microkelvin Platform (H2020 project 824109), and the European Research Council (ERC Advanced Grant 101055088, CorMeTop). The work in Prague was supported by the Czech Science Fund (GAČR project No. 19-29614L). M.G.V. acknowledges support to the Spanish Ministerio de Ciencia e Innovación (grant PID2022-142008NB-I00), partial support from European Research Council (ERC) grant agreement no. 101020833 and the European Union NextGenerationEU/PRTR-C17.I1, as well as by the IKUR Strategy under the collaboration agreement between Ikerbasque Foundation and DIPC on behalf of the Department of Education of the Basque Government. D.-G.O., C.F., R.V., and M.G.V. acknowledge funding from the German Research Foundation (DFG) and the Austrian Science Fund (FOR 5249 - QUAST).

Appendix A: Materials and Methods

Appendix B: Structure refinement from powder and single crystal X-ray diffraction

Appendix C: Relationship between stoichiometry, structural, and magnetic susceptibility data

Appendix D: Density functional theory (DFT) calculations

---

[1] M. Dzero, J. Xia, V. Galitski, and P. Coleman, Topological Kondo insulators, Annu. Rev. Condens. Matter Phys. **7**, 249 (2016).

[2] L. Li, K. Sun, C. Kurdak, and J. W. Allen, Emergent mystery in the Kondo insulator samarium hexaboride, Nat. Rev. Phys. **2**, 463 (2020).

[3] S. Paschen and Q. Si, Quantum phases driven by strong correlations, Nat. Rev. Phys. **3**, 9 (2021).

[4] Z. Fisk, J. D. Thompson, and H. R. Ott, Heavy-electrons: new materials, J. Magn. Magn. Mater. **76-77**, 637 (1988).

[5] M. F. Hundley, P. C. Canfield, J. D. Thompson, Z. Fisk, and J. M. Lawrence, Hybridization gap in $Ce_3Bi_4Pt_3$, Phys. Rev. B **42**, 6842 (1990).

[6] Z. Fisk, P. C. Canfield, J. D. Thompson, and M. F. Hundley, $Ce_3Bi_4Pt_3$ and hybridization Gap physics, J. of Alloys and Compounds **181**, 369 (1992).

[7] P. S. Riseborough, Heavy fermion semiconductors, Adv. Phys. **49**, 257 (2000).

[8] S. Dzsaber, L. Prochaska, A. Sidorenko, G. Eguchi, R. Svagera, M. Waas, A. Prokofiev, Q. Si, and S. Paschen, Kondo insulator to semimetal transformation tuned by spin-orbit coupling, Phys. Rev. Lett. **118**, 246601 (2017).

[9] H.-H. Lai, S. E. Grefe, S. Paschen, and Q. Si, Weyl-Kondo semimetal in a heavy fermion system, Proc. Natl. Acad. Sci. U.S.A. **115**, 93 (2018).

[10] S. Dzsaber, X. Yan, G. Eguchi, A. Prokofiev, T. Shiroka, P. Blaha, O. Rubel, S. E. Grefe, H.-H. Lai, Q. Si, and S. Paschen, Giant spontaneous Hall effect in a nonmagnetic Weyl-Kondo semimetal, Proc. Natl. Acad. Sci. U.S.A. **118**, e2013386118 (2021).

[11] S. Dzsaber, D. A. Zocco, A. McCollam, F. Weickert, R. McDonald, M. Taupin, G. Eguchi, X. Yan, A. Prokofiev, L. M. K. Tang, B. Vlaar, L. E. Winter, M. Jaime, Q. Si, and S. Paschen, Control of electronic topology in a strongly correlated electron system, Nat. Commun. **13**, 5729 (2022).

[12] S. E. Grefe, H.-H. Lai, S. Paschen, and Q. Si, Weyl-Kondo semimetal: Towards control of Weyl nodes, JPS Conf. Proc. **30**, 011013 (2020).

[13] S. E. Grefe, H.-H. Lai, S. Paschen, and Q. Si, Extreme topological tunability of Weyl-Kondo semimetal to Zeeman coupling, arXiv:2012.15841 (2021).

[14] S. K. Kushwaha, M. K. Chan, J. Park, S. M. Thomas, E. D. Bauer, J. D. Thompson, F. Ronning, P. F. S. Rosa, and N. Harrison, Magnetic field-tuned Fermi liquid in a Kondo insulator, Nat. Commun. **10**, 5487 (2019).

[15] M. O. Ajeesh, S. M. Thomas, S. K. Kushwaha, E. D. Bauer, F. Ronning, J. D. Thompson, N. Harrison, and P. F. S. Rosa, Ground state of $Ce_3Bi_4Pd_3$ unraveled by hydrostatic pressure, Phys. Rev. B **106**, L161105 (2022).

[16] J. M. Tomczak, Isoelectronic tuning of heavy fermion systems: Proposal to synthesize $Ce_3Sb_4Pd_3$, Phys. Rev. B **101**, 035116 (2020).

[17] C. Xu, C. Cao, and J.-X. Zhu, Pressure-induced concomitant topological and metal-insulator quantum phase transitions in $Ce_3Pd_3Bi_4$, npj Quantum Mater. **7**, 18 (2022).

[18] S.-K. Zhang, Y.-J. Xu, C.-E. Hu, Y. Cheng, J. Zhu, and G.-F. Ji, Pressure-driven change of ground state of $Ce_3Pd_3Bi_4$: A DFT+DMFT study, Phys. Rev. B **106**, 205115 (2022).

[19] A. E. Dwight, Yttrium–gold–antimony $Y_3Au_3Sb_4$, Acta Cryst. B **33**, 1579 (1977).

[20] A. E. Dwight, Crystal structure of $U_3Ni_3Sb_4$ and related compounds, J. Nucl. Mater. **79**, 417 (1979).

[21] T. Takabatake, S.-i. Miyata, H. Fujii, Y. Aoki, T. Suzuki, T. Fujita, J. Sakurai, and T. Hiraoka, Heavy-Fermion and Semiconducting Properties of the Ternary Uranium Compounds $U_3T_3Sn_4$ and $U_3T_3Sb_4$ (T = Ni, Cu, Pd, Pt and Au), J. Phys. Soc. Jpn. **59**, 4412 (1990).

[22] M. Wang, R. McDonald, and A. Mar, $M_3Ni_3Sb_4$ (M = Zr, Hf) and $Zr_3Pt_3Sb_4$. Ternary Antimonides with the $Y_3Au_3Sb_4$ Structure, Inorg. Chem. **38**, 3435 (1999).

[23] W. B. Pearson, *The crystal chemistry and physics of metals and alloys*, Wiley series on the science and technology of materials (Wiley - Interscience, New York, USA, 1972).

[24] P. Coleman, $\frac{1}{N}$ expansion for the Kondo lattice, Phys. Rev. B **28**, 5255 (1983).

[25] T. Takabatake, F. Iga, T. Yoshino, Y. Echizen, K. Katoh, K. Kobayashi, M. Higa, N. Shimizu, Y. Bando, G. Nakamoto, H. Fujii, K. Izawa, T. Suzuki, T. Fujita, M. Sera, M. Hiroi, K. Maezawa, S. Mock, H. v. Löhneysen, A. Brückl, K. Neumaier, and K. Andres, Ce- and Yb-based Kondo semiconductors, J. Magn. Magn. Mater. **177-181**, 277 (1998).

[26] C. Kittel, *Introduction to Solid State Physics*, 8th ed. (Wiley, 2004).

[27] In Ref. [15], the values of activated energy, which amount to half of the total energy gap Δ used here, were obtained from Arrhenius fits. For example, the authors reported an activated energy of 28 K at 2.3 GPa, which is equivalent to an energy gap of 56 K $\sim$ 4.8 meV.

[28] F. Birch, Finite elastic strain of cubic crystals, Phys. Rev. **71**, 809 (1947).

[29] D. J. Campbell, Z. E. Brubaker, C. Roncaioli, P. Saraf, Y. Xiao, P. Chow, C. Kenney-Benson, D. Popov, R. J. Zieve, J. R. Jeffries, and J. Paglione, Pressure-driven valence increase and metallization in the Kondo insulator $Ce_3Bi_4Pt_3$, Phys. Rev. B **100**, 235133 (2019).